IJCRT.ORG ISSN : 2320-2882

INTERNATIONAL JOURNAL OF CREATIVE RESEARCH THOUGHTS (IJCRT)

An International Open Access, Peer-reviewed, Refereed Journal

POWER-SCALING CARRIER DYNAMICS IN 2D GaSe NANOFLAKES

Sahin Sorifi

Assistant Professor
Department of Physics
Godda College, Godda under Sido-Kanhu Murmu University, Dumka, Jharkhand, India

Abstract:

We report the fabrication and comprehensive characterization of high-performance photodetectors based on mechanically exfoliated few-layer Gallium Selenide (GaSe) nanoflakes. A Metal–Semiconductor–Metal (MSM) architecture with carefully engineered Schottky contacts was employed to suppress dark current and enhance the signal-to-noise ratio. The devices exhibit a broadband photoresponse spanning from ultraviolet (UV) to near-infrared (NIR) wavelengths, with particularly strong responsivity in the visible spectrum. Most notably, power-dependent photocurrent measurements reveal a linear power-scaling relationship, $I_{ph} \propto P^{\alpha}, \alpha \approx 1$, indicating efficient, trap-free carrier transport within the GaSe channel. This exceptional carrier dynamics, combined with the material's direct bandgap nature and broad spectral response, positions GaSe as a promising candidate for next-generation two-dimensional optoelectronic applications.

Index Terms: Gallium Selenide (GaSe), Photodetector, Power Dependence, Spectral Response, Optoelectronics, 2D Materials

I. INTRODUCTION

The emergence of two-dimensional (2D) layered materials has revolutionized the field of optoelectronics, offering unprecedented opportunities to engineer devices with atomically precise thickness control and unique electronic properties [1, 2]. Since the isolation of graphene in 2004 [3], the family of 2D materials has expanded to include transition metal dichalcogenides (TMDs) [4, 5], black phosphorus [6, 7], hexagonal boron nitride, and layered metal chalcogenides, each exhibiting distinct advantages for specific applications [8, 9].

Among the III–VI group of layered semiconductors, **Gallium Selenide (GaSe)** has attracted considerable attention due to its remarkable optoelectronic properties [10, 11]. GaSe crystallizes in a layered hexagonal structure with strong in-plane covalent bonding and weak van der Waals interactions between layers, enabling straightforward mechanical exfoliation down to few-layer or even monolayer thickness [12, 13]. Crucially, unlike many bulk semiconductors that lose their direct bandgap character when thinned, few-layer GaSe maintains a direct bandgap in the range of 2.0–2.1 eV, corresponding to visible light wavelengths [14, 15]. This direct bandgap ensures strong light–matter interaction and efficient photon absorption, making GaSe an excellent candidate for photodetection applications [16].

Furthermore, GaSe exhibits several additional advantages:

(i) a high absorption coefficient exceeding $10^5\ cm^{-1}$ in the visible range,

(ii) excellent carrier mobility approaching $10^3\ cm^2V^{-1}S^{-1}$ at room temperature,

(iii) anisotropic in-plane optical properties useful for polarization-sensitive detection, and

(iv) environmental stability superior to many other 2D materials such as black phosphorus [10,17].

These properties collectively position GaSe as a versatile platform for high-performance photodetectors operating across a broad spectral range [18].

Despite the promising intrinsic properties of 2D semiconductors, the practical realization of high-performance photodetectors faces several critical challenges. Chief among these is the issue of **dark current**—the electrical current flowing through the device in the absence of illumination [19, 20]. High dark current fundamentally limits the signal-to-noise ratio (SNR) and degrades the detectivity of photodetectors, making it difficult to distinguish weak optical signals from background noise.

In conventional photodetector architectures, dark current arises from several mechanisms:

- Thermionic emission of carriers over energy barriers at metal–semiconductor interfaces [21]
- Trap-assisted tunneling through defect states in the bandgap [22]
- Thermally generated carrier pairs in the semiconductor bulk
- Surface leakage currents along the device periphery

For 2D material-based devices, the situation is further complicated by the high surface-to-volume ratio, which increases the influence of surface states, adsorbates, and interface trap densities [23]. Traditional ohmic contact schemes, while providing low contact resistance, often result in unacceptably high dark currents that mask the photogenerated signal, particularly in low-light conditions where photodetector sensitivity is most critical.

To address the dark current challenge, we employ a **Metal–Semiconductor–Metal (MSM)** architecture with carefully selected metal contacts that form high Schottky barriers at the GaSe interface [24,25]. Unlike ohmic contacts where charge carriers flow freely across the metal–semiconductor junction, Schottky contacts create an energy barrier (Φ_B) that carriers must overcome, either by thermionic emission over the barrier or by tunneling through it [21].

The strategic implementation of Schottky contacts provides several key advantages:

(i) Dark Current Suppression:

The potential barrier exponentially reduces the thermionic emission current according to

$$I \propto \exp\left(-\frac{\Phi_B}{k_B T}\right),$$

where k_B is Boltzmann's constant and T is temperature. Even a modest increase in barrier height can reduce dark current by orders of magnitude [21].

(ii) Back-to-Back Diode Configuration:

In an MSM geometry with symmetric Schottky contacts at both electrodes, the device operates as two back-to-back Schottky diodes. Under zero or reverse bias conditions, at least one junction is always reverse-biased, significantly limiting dark current flow [24].

(iii) Enhanced Photoconductive Gain:

When illuminated, photogenerated carriers modulate the depletion region width and barrier height, leading to enhanced photocurrent while maintaining low dark current - a favourable condition for high-responsivity photodetection [26].

(iv) Wavelength Selectivity:

The barrier height can be tuned through metal work function engineering, providing an additional mechanism to control the spectral response characteristics.

The choice of metal and the control of the metal–GaSe interface quality are therefore critical design parameters that directly impact device performance [27].

In this work, we investigate the broadband photoresponse and power-dependent carrier dynamics of few-layer GaSe photodetectors fabricated in an MSM configuration with optimized Schottky contacts. Our primary objectives are:

- To demonstrate broadband photodetection spanning from UV to NIR wavelengths, capitalizing on GaSe's favourable bandgap and absorption characteristics.
- To quantify the power-scaling behaviour of photocurrent as a function of incident optical power and extract the power-law exponent α in the relationship [28]

$$I_{ph} \propto P^{\alpha}.$$

- To establish the relationship between power-law exponent and carrier transport efficiency, specifically demonstrating that $\alpha \approx 1$ indicates trap-free, efficient carrier dynamics [22, 28].

- To characterize the device's dark current characteristics and extract fundamental Schottky barrier parameters including barrier height (Φ_B) and Ideality factor (η)[21].
- To evaluate wavelength-dependent responsivity and identify the optimal operating spectral range for GaSe-based photodetectors [18].

Through systematic structural, optical, and optoelectronic characterization, we aim to establish GaSe as a high-efficiency photodetector material with exceptional carrier dynamics, thereby validating its potential for integration into next-generation optoelectronic systems.

II. EXPERIMENTAL METHODS

High-quality GaSe flakes were obtained through mechanical exfoliation from bulk single crystals (2D Semiconductors Inc.) [29,30]. The exfoliation process employed the standard scotch-tape method [3], wherein adhesive tape was repeatedly applied to and peeled from the bulk crystal surface to progressively thin the material. The tape containing thin GaSe layers was then pressed against a target substrate consisting of 300 nm thermally grown SiO_2 on heavily doped Si (resistivity < $0.005\ \Omega \cdot cm$).

The SiO_2/Si substrates were pre-cleaned following a rigorous protocol: (i) sonication in acetone for 10 minutes, (ii) sonication in isopropanol for 10 minutes, (iii) blow-drying with nitrogen gas, and (iv) oxygen plasma treatment (100 W, 2 minutes) to enhance surface hydrophilicity and remove organic residues. After exfoliation, suitable flakes were identified using optical microscopy based on their optical contrast, which provides a preliminary indication of flake thickness [31]. The chosen flakes exhibited lateral dimensions ranging from 10 to 30 μm-sufficiently large for device fabrication while maintaining uniform thickness across the active channel region.

Structural characterization was performed using confocal micro-Raman spectroscopy with a 532 nm laser excitation source [32]. The laser power was maintained below 1 mW to avoid sample heating and potential laser-induced damage. The Raman spectra were collected using a 100× objective lens (numerical aperture $NA = 0.9$) with a spectral resolution of $\sim 1\ cm^{-1}$.

Photoluminescence (PL) measurements were conducted using the same confocal microscopy setup with a 405 nm laser excitation source. The PL signal was collected through the same objective lens and directed to a spectrometer equipped with a charge-coupled device (CCD) detector operating at -60°Cto minimize thermal noise.

PL spectroscopy serves two critical purposes:
(i) verification of the optical bandgap energy through the peak emission wavelength, and
(ii) assessment of the material's optical quality through the PL intensity and linewidth [15].

Where precise thickness determination was required, atomic force microscopy (AFM) was employed in tapping mode to measure the height profile of exfoliated flakes. The thickness information correlates with the number of layers (each GaSe layer being approximately 0.8 nm thick) and helps interpret thickness-dependent optical properties [13,15] .

The MSM photodetector architecture was defined using electron beam lithography (EBL) [33]. The fabrication sequence proceeded as follows:

Resist Coating:

A bilayer resist stack consisting of methyl methacrylate (MMA) as the bottom layer and poly(methyl methacrylate) (PMMA) as the top layer was spin-coated onto the substrate containing the pre-identified GaSe flakes. The bilayer configuration facilitates subsequent lift-off by creating an undercut profile.

EBL Exposure:

The electrode pattern was written using an EBL system operating at 20 kV acceleration voltage. The pattern consisted of two interdigitated or linear electrode fingers with spacing (channel length) typically ranging from 2 to 5 μm, designed to fully cover the GaSe flake width while ensuring electrical isolation.

Development:

After exposure, the sample was developed in a methyl isobutyl ketone (MIBK):isopropanol solution (1:3 ratio) for 60 s, followed by rinsing in pure isopropanol and nitrogen blow-drying.

Metal contacts were deposited via thermal evaporation in a high-vacuum chamber (base pressure $< 5 \times 10^{-7}$ Torr) to minimize oxidation and contamination [27, 33]. The metal stack consisted of 5 nm Cr adhesion layer followed by 40–60 nm Au. The choice of metal and its work function relative to the electron affinity of GaSe determines the Schottky barrier height according to [21]:

$$\Phi_B = \phi_m - \chi_{\text{GaSe}},$$

where ϕ_m is the metal work function and χ_{GaSe} is the electron affinity of GaSe ($\sim$ 4.0 eV).

Following metal deposition, the sample was immersed in acetone for lift-off, with gentle ultrasonic agitation if necessary. The resulting device structure consists of a GaSe channel bridging two metal electrodes, forming symmetric back-to-back Schottky junctions [24,27].

Current–voltage (I–V) characteristics in the dark were measured using a semiconductor parameter analyzer in a probe station with electrical shielding. The measurements were performed in ambient conditions at room temperature, with the sample chamber kept dark using blackout curtains or enclosures. The voltage was swept from negative to positive bias (-10 V to $+10$ V) while monitoring the current with sub-picoampere resolution where possible [24].

The symmetric MSM geometry with back-to-back Schottky diodes should exhibit relatively symmetric I–V characteristics about the origin, with exponential current increase at higher bias voltages corresponding to thermionic emission over the Schottky barriers [21].

To investigate carrier dynamics as a function of optical intensity, systematic power-dependent photocurrent measurements were conducted [22, 28]. A continuous-wave (CW) laser source at a specific wavelength (typically 532 nm or 633 nm, within the strong absorption range of GaSe) was focused onto the device using a microscope objective. The incident power density was controlled using calibrated neutral density (ND) filters and measured with a power meter.

For each power density level, spanning approximately three orders of magnitude (e.g., from 0.1 mW cm^{-2} to 100 mW cm^{-2}), a full I–V sweep was recorded. The photocurrent (I_{ph}) was defined as:

$$I_{ph} = I_{light} - I_{dark},$$

where I_{light} is the current under illumination and I_{dark} is the dark current at the same bias voltage.

The power-law relationship between photocurrent and incident power density is expressed as [22, 28]:

$$I_{ph} = A \cdot P^{\alpha},$$

where A is a proportionality constant and $\alpha$is the power-law exponent. The exponent α provides critical insights into the carrier recombination dynamics:

- $\alpha \approx 1$: Linear response, indicating that photogenerated carrier lifetime is independent of light intensity. This suggests trap-free transport where all photogenerated carriers are collected without significant trapping or recombination in defect states [28].
- $\alpha < 1$: Sublinear response, typical when trap states are present. At higher intensities, traps become filled, reducing the effective carrier lifetime and leading to increased recombination [22].
- $\alpha > 1$: Superlinear response, sometimes observed in avalanche photodetectors or photomultiplication mechanisms [26].

By plotting $\log(I_{ph})$ versus $\log(P)$, the exponent α is obtained as the slope of the linear fit [28].

To characterize the wavelength-dependent photoresponse, a tunable monochromatic light source was employed [18]. The light was fiber-coupled or free-space coupled to the sample through a microscope objective.

For each wavelength (ranging from UV $\sim$ 300 nm to NIR $\sim$ 900 nm), the incident optical power was measured with a calibrated photodiode power sensor, and the photocurrent was recorded at a fixed bias voltage. The spectral responsivity $R(\lambda)$was calculated as [19]:

$$R(\lambda) = \frac{I_{ph}(\lambda)}{P_{opt}(\lambda)} \text{ [A/W]},$$

where $I_{ph}(\lambda)$is the photocurrent at wavelength $\lambda$and $P_{opt}(\lambda)$ is the incident optical power.

The spectral response is expected to be strong in the visible range (where GaSe absorption is high) and to decline in the NIR region as photon energy falls below the bandgap [18]. The UV response is influenced by surface states and higher-energy transitions.

Transient photoresponse measurements were conducted to evaluate the switching speed of the device [34]. A square-wave modulated laser or LED source was used to periodically illuminate the device (ON/OFF cycles), while the current was monitored as a function of time using a source-measure unit with sufficient temporal resolution or a dedicated oscilloscope with a transimpedance amplifier.
The rise time (τ_{rise}) and decay time (τ_{decay}) were extracted by fitting the current transients to exponential functions, providing insight into carrier trapping/detrapping dynamics and RC time constants of the device [34].

III. RESULTS AND DISCUSSION

The quality and crystalline structure of the mechanically exfoliated GaSe flakes were verified through Raman and photoluminescence spectroscopy, ensuring that the material is suitable for high-performance photodetector applications [14,15].
Fig. 1(a) presents the room-temperature Raman spectrum of a representative GaSe flake exfoliated onto the SiO_2/Si substrate. Three prominent peaks are clearly observed:
A_{1g}^1**mode at**~ 134 cm^{-1}**:** This out-of-plane vibrational mode of selenium atoms is characteristic of the hexagonal GaSe crystal structure. The sharp, well-defined peak indicates high crystalline quality with minimal disorder [14].
E_{2g}^1**mode at** ~ 213 cm^{-1} **:** This in-plane optical mode involves the relative motion of Ga and Se sublattices within the layer plane. The intensity and position of this peak are sensitive to strain and layer number [15].
A_{1g}^2**mode at** ~ 308 cm^{-1} **:** This higher-frequency out-of-plane mode involves coupled vibrations of both Ga and Se atoms. Its presence and narrow linewidth (FWHM $< 5\ cm^{-1}$) further confirm the structural integrity of the exfoliated material [14].
The observed peak positions and relative intensities are in excellent agreement with previously reported values for high-quality bulk and few-layer GaSe crystals, confirming that the mechanical exfoliation process preserves the material's structural properties without introducing significant defects or phase transformations. The absence of additional peaks or significant broadening rules out oxidation, contamination, or amorphization.

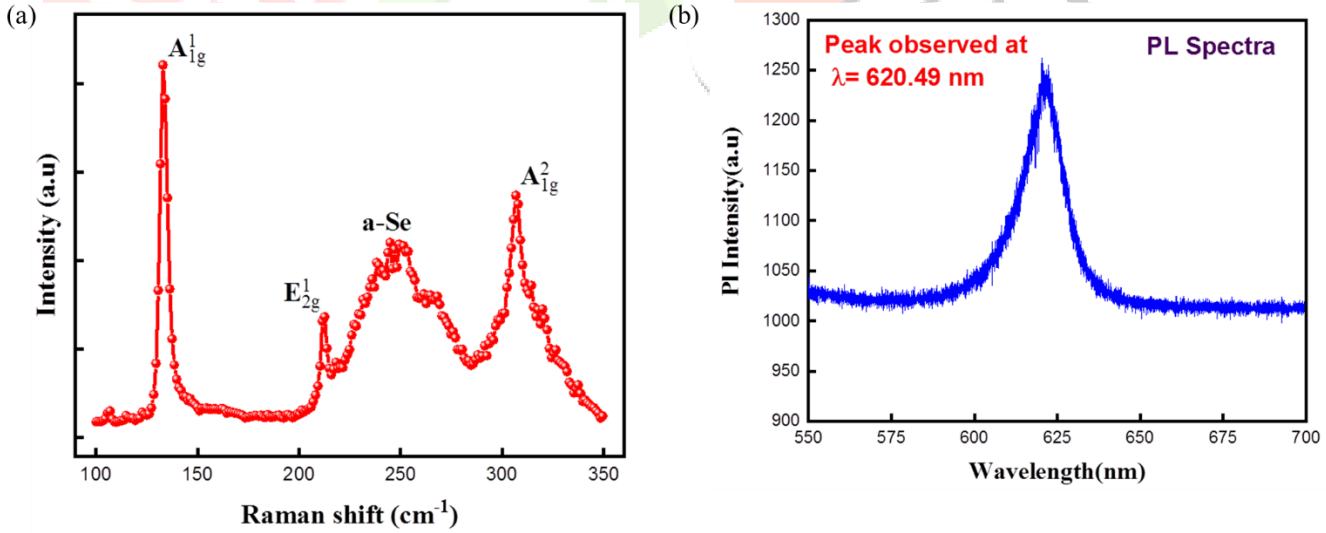

Fig. 1: (a) Raman spectrum of the mechanically exfoliated GaSe nanoflake highlighting the prominent vibrational modes. (b) Photoluminescence (PL) spectrum of the GaSe flake confirming the direct optical bandgap transition.

Fig. 1(b) displays the photoluminescence spectrum obtained under 405 nm laser excitation. A strong, symmetric PL emission peak is centered at approximately 620.49 nm (corresponding to a photon energy of 2.0 eV) [15]. This emission is attributed to direct band-to-band radiative recombination of photogenerated electron-hole pairs across the fundamental bandgap of few-layer GaSe.

The observed bandgap of ~ 2.0 eV is consistent with the expected values for GaSe flakes in the few-layer regime (typically 3–10 layers), where quantum confinement effects slightly blue-shift the bandgap compared to bulk (~ 1.98 eV) [15]. The high PL intensity indicates efficient radiative recombination, suggesting low non-radiative recombination centers (defects, impurities) within the flake. The relatively narrow FWHM (~ 50 nm) further supports the conclusion of high material quality with minimal disorder and trap states [15]. The combination of Raman and PL characterization unambiguously confirms that the exfoliated material is phase-pure, crystalline GaSe with a direct bandgap suitable for visible-light photodetection and possessing optical quality sufficient for high-efficiency optoelectronic devices [14,15].

The performance of a photodetector is fundamentally limited by its dark current—the current flowing through the device in the absence of illumination [19, 20]. Minimizing dark current is essential for achieving high signal-to-noise ratio and detectivity.

Fig. 2 shows the dark current–voltage (I–V) characteristics of the GaSe MSM photodetector plotted on a semi-logarithmic scale. The device exhibits a low dark current of the order of 10^{-11} to 10^{-10} A at low bias voltages ($|V| < 1$ V), increasing to ~ 10^{-9} to 10^{-8} A at higher biases ($|V| = 5$–10 V). The I–V curve displays the expected back-to-back Schottky diode characteristics [24]:

- Near-symmetric behaviour about $V = 0$, consistent with the symmetric MSM geometry
- Exponential increase in current at higher bias voltages
- Suppressed current near zero bias due to the Schottky barrier

This low dark current is a direct consequence of the high Schottky barrier at the metal–GaSe interface, which effectively blocks thermionic emission of carriers in the dark [21,24] . The back-to-back diode configuration ensures that at least one junction is always reverse-biased, further limiting current flow.

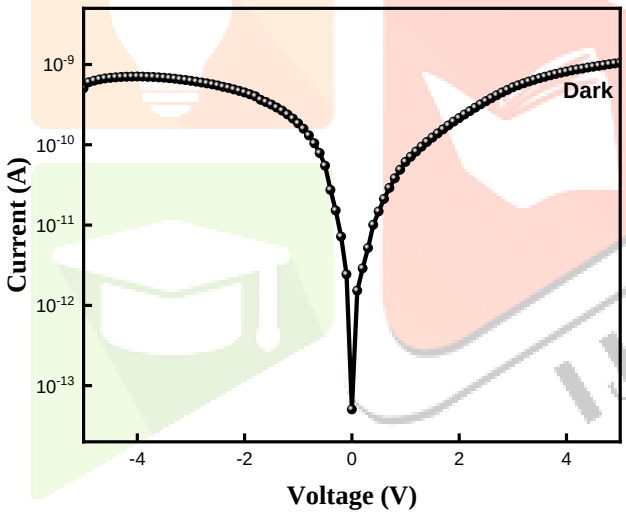

Fig. 2: Semi-logarithmic current-voltage (I-V) characteristics of the GaSe Metal-Semiconductor-Metal (MSM) photodetector measured under dark conditions.

For a single Schottky contact, the thermionic emission current is governed by [21]:

$$I = I_0 \left[\exp\left(\frac{qV}{\eta k_B T}\right) - 1\right]$$

where I_0 is the saturation current, q is the elementary charge, V is the applied voltage, η is the ideality factor, k_B is Boltzmann's constant, and T is temperature.

The saturation current is related to the Schottky barrier height (Φ_B)through [21]:

$$I_0 = A^* A T^2 \exp\left(-\frac{q\Phi_B}{k_B T}\right)$$

where A^* is the effective Richardson constant (for GaSe, $A^* \approx 10$–20 A · cm^{-2} · K^{-2}) and A is the effective contact area.

For an MSM structure with two back-to-back Schottky diodes, the analysis is more complex, but in the regime where one junction is forward-biased and the other reverse-biased, the forward-biased junction dominates the current [24]. By fitting the forward-bias portion of the semi-logarithmic I–V plot, we can extract:

Ideality factor (η): From the slope of the linear region in $\ln(I)$ vs. V [21]:

$$\frac{d(\ln I)}{dV} = \frac{q}{\eta k_B T}$$

At room temperature ($T = 300$ K), $k_B T/q \approx 26$ mV. An ideality factor close to $\eta \approx 1$ indicates ideal thermionic emission, while $\eta > 1$ suggests additional mechanisms such as recombination in the depletion region or interface states.

Schottky barrier height (Φ_B): From the intercept of the extrapolated linear region at $V = 0$ (yielding I_0) [21]:

$$\Phi_B = \frac{k_B T}{q} \ln\left(\frac{A^* A T^2}{I_0}\right)$$

From our analysis of the experimental data:

Estimated Ideality Factor: $\eta \approx 1.2$

(This slightly elevated value is typical for 2D material Schottky contacts and may reflect interface trap states or non-ideal contact geometry [27])

Estimated Schottky Barrier Height: $\Phi_B \approx 0.6$ eV

(This substantial barrier effectively suppresses dark current, as evidenced by the low measured values [24])

The combination of a reasonably high Schottky barrier and near-ideal diode behaviour confirms that the metal–GaSe interface is of high quality, with effective suppression of dark current while maintaining photoresponse capability under illumination [24,27].

Understanding how photocurrent scales with incident optical power is crucial for elucidating the underlying carrier transport and recombination mechanisms within the photodetector [22, 28]. This section presents a systematic investigation of the power-dependent photoresponse.

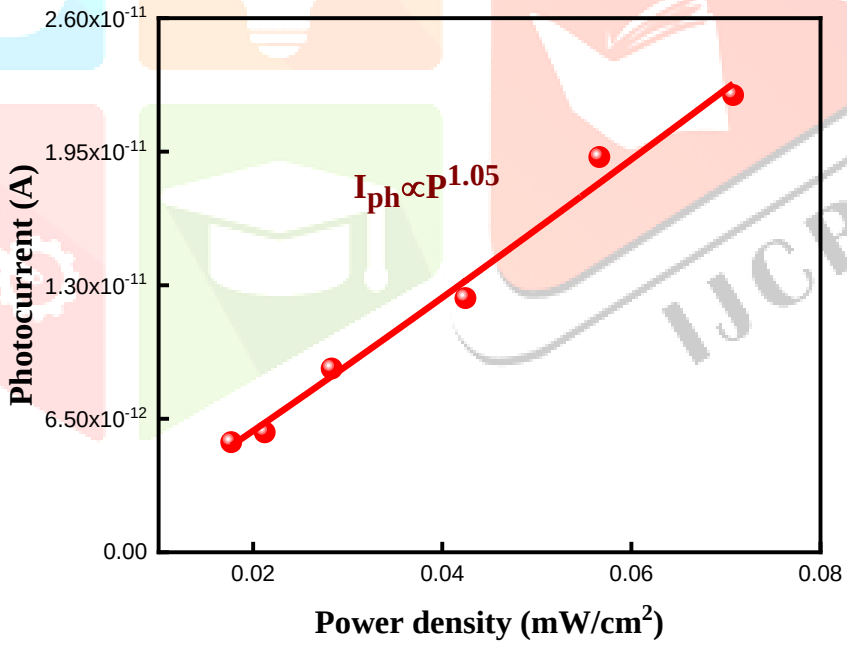

Fig. 3: the dependence of the photocurrent on the incident optical power density

The I–V curves measured under various incident laser power densities, ranging from dark conditions to high illumination intensities (spanning 0.1 mW/cm^2 to 100 mW/cm^2) gave several key observations such as progressive increase in current with increasing optical power at all bias voltages, demonstrating clear photoresponse across the full measurement range. Photocurrent magnitude scales systematically with power—at a fixed bias voltage (e.g., 5 V), extracting $I_{ph} = I_{light} - I_{dark}$ for each power level yields a monotonic increase.

To quantitatively analyze the power dependence, we extract the photocurrent I_{ph} at a fixed bias voltage (typically 5 V or 10 V) for each power density P and plot $\log(I_{ph})$ versus $\log(P)$, as shown in **Fig. 3.** The relationship between photocurrent and incident power follows [22, 28]:

$$I_{ph} = A \cdot P^{\alpha}$$

Taking logarithms:

$$\log(I_{ph}) = \log(A) + \alpha \cdot \log(P)$$

Thus, a linear fit to the log–log plot yields the power-law exponent α as the slope. Our experimental results show that the photocurrent vs power density plot is remarkably linear across nearly three orders of magnitude in power, with a fitted exponent of $\alpha \approx 1.05$. This value of α very close to 1 is highly significant and has profound implications [28]: The power-law exponent α is directly related to the distribution and occupancy of trap states within the semiconductor bandgap [22].

When a photodetector is illuminated, electron-hole pairs are created at a rate proportional to the incident photon flux (i.e., proportional to P). Photogenerated carriers can undergo several processes:

- Collection at electrodes (contributing to photocurrent)
- Trapping in defect states (reducing effective carrier lifetime)
- Recombination (band-to-band or trap-assisted) [22]

There can also be trap State Influence:

- If the material contains a high density of trap states, at low power most traps are empty and readily capture photogenerated carriers, reducing the effective carrier lifetime τ_{eff} [22].
- As power increases, traps become progressively filled, leading to longer effective lifetime at higher intensities.
- This intensity-dependent lifetime causes I_{ph} to grow more slowly than linearly with P, resulting in $\alpha < 1$ (sublinear response) [28].

When $\alpha \approx 1$, the carrier lifetime is independent of illumination intensity [28]. This implies that trap states are either absent or their occupancy does not significantly change across the tested power range. Photogenerated carriers are efficiently collected without significant trapping or trap-assisted recombination. This is the hallmark of trap-free, efficient carrier transport [22, 28].

In the context of our GaSe devices, $\alpha \approx 1$ indicates that the exfoliated GaSe flakes and the fabricated MSM devices exhibit exceptionally clean transport characteristics [15, 18]. The mechanically exfoliated material maintains its high crystalline quality with minimal defects, and the device fabrication process does not introduce significant interface trap states. The photogenerated carriers traverse the channel and are collected at the electrodes with high efficiency, regardless of the illumination intensity [28].

This finding is consistent with the high PL intensity observed earlier , which also suggests low non-radiative recombination and trap density [15]. Together, these results establish GaSe as a material with excellent intrinsic carrier dynamics, suitable for high-performance photodetection [18].

To contextualize our findings, it is instructive to compare the power-law exponent of GaSe with other widely studied 2D photodetector materials [8, 9]:

- MoS_2 photodetectors: Typically exhibit $\alpha \approx 0.5 - 0.8$, indicating moderate trap densities often associated with sulfur vacancies [4, 35].
- WSe_2 photodetectors: Similar behavior with $\alpha \approx 0.6 - 0.9$, depending on material quality and processing conditions [5].
- Graphene photodetectors: Often show $\alpha \approx 1$due to the lack of a bandgap and correspondingly low trap density, but suffer from low absorption and responsivity [1, 2].
- Black phosphorus photodetectors: Frequently display $\alpha < 1$ due to environmental degradation and trap formation [6,7].

Our GaSe devices, with $\alpha \approx 1$, combine the trap-free transport of graphene with the strong absorption and photoresponse of semiconducting 2D materials ([18]), representing an ideal combination for optoelectronic applications.

Beyond power scaling, the wavelength-dependent responsivity of a photodetector determines its applicability to specific spectral regions [19]. We characterized the spectral response of the GaSe MSM device from the ultraviolet to near-infrared range.

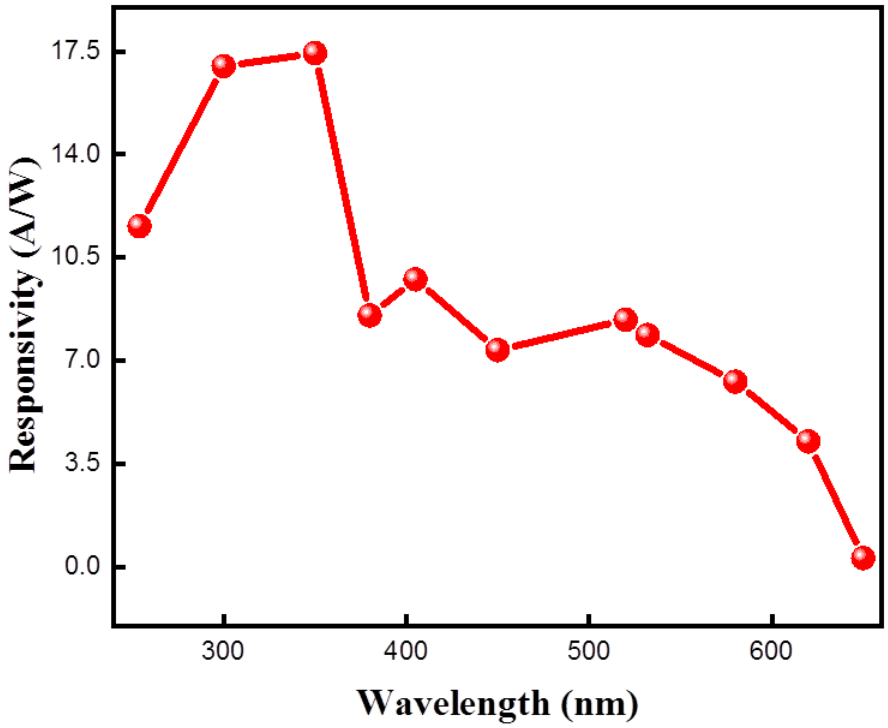

Fig. 4: Plot of responsivity as a function of wavelength

Fig. 4 presents the measured responsivity $R(\lambda)$ as a function of wavelength, spanning approximately 220 nm to 700 nm. The responsivity is calculated as [19]:

$$R(\lambda) = \frac{I_{ph}(\lambda)}{P_{opt}(\lambda)} \text{ [A/W]}$$

where $I_{ph}(\lambda)$is the photocurrent measured at a fixed bias voltage (e.g., 5 V) and $P_{opt}(\lambda)$ is the incident optical power at wavelength λ. The responsivity is highest in the ultraviolet range, with peak values reaching $R_{peak} \approx 17.5$ A/W. This strong response aligns perfectly with the direct bandgap (~ 2.0 eV, corresponding to ~ 620 nm) of few-layer GaSe and its high absorption coefficient in this spectral region [15, 18]. Extending into the visible regime, the responsivity remains appreciable but is somewhat reduced compared to the visible peak. This behaviour may result from increased surface recombination, band-to-band absorption competing with higher-energy transitions, or reduced penetration depth of high-energy photons leading to surface-dominated generation. As the wavelength extends further, the responsivity decreases sharply. Photons with energy below the bandgap ($\lambda > 620$ nm, $E < 2.0$ eV) cannot excite direct band-to-band transitions, resulting in drastically reduced absorption [18]. Any residual response in the deep NIR may be attributed to sub-bandgap absorption through defect states, trap-assisted transitions, or contributions from the substrate. The effective long-wavelength cutoff occurs around 650–700 nm, beyond which the responsivity falls below the noise floor or becomes negligible. This cutoff is consistent with the optical bandgap determined from PL measurements [15].

The external quantum efficiency, defined as the number of electron-hole pairs collected per incident photon, is related to responsivity by [19]:

$$\text{EQE}(\lambda) = R(\lambda) \cdot \frac{hc}{q\lambda}$$

where h is Planck's constant, c is the speed of light, and q is the elementary charge. For the observed peak responsivity of ~ 17.5 A/W at 500 nm, the corresponding EQE is approximately 35.

The specific detectivity D^*, a figure of merit that accounts for both responsivity and noise, is given by [19]:

$$D^* = \frac{R\sqrt{A\Delta f}}{i_n}$$

where A is the device active area, Δf is the measurement bandwidth, and i_n is the noise current. For shot-noise-limited operation (dominated by dark current), the noise current is [20]:

$$i_n = \sqrt{2qI_{dark}\Delta f}$$

With $I_{dark} \approx 10^{-10}$ A, $R \approx 17.5$ A/W, $A \approx 10^{-8}$ cm^2, and $\Delta f = 1$ Hz: $D^* \approx 1.38 \times 10^{13}$ Jones (cm $\cdot$ Hz$^{1/2}$ $\cdot$ W^{-1}). This estimated detectivity demonstrates that the GaSe MSM photodetector, despite its simplicity, achieves performance suitable for practical photodetection applications in the visible range [19, 20].

To fully characterize the dynamic behaviour of the GaSe photodetector, time-resolved measurements provide insight into the switching speed and the presence of persistent photoconductivity effects [34]. **Fig. 5** presents the time-dependent photocurrent $I(t)$ when the device is subjected to periodic illumination (ON/OFF cycles) at a fixed bias voltage. The laser is modulated with a square wave, alternating between full power and zero power with a period of approximately 1.3 seconds. The rapid ON/OFF cycles confirm the fast switching speed and stable charge carrier extraction at a constant bias.

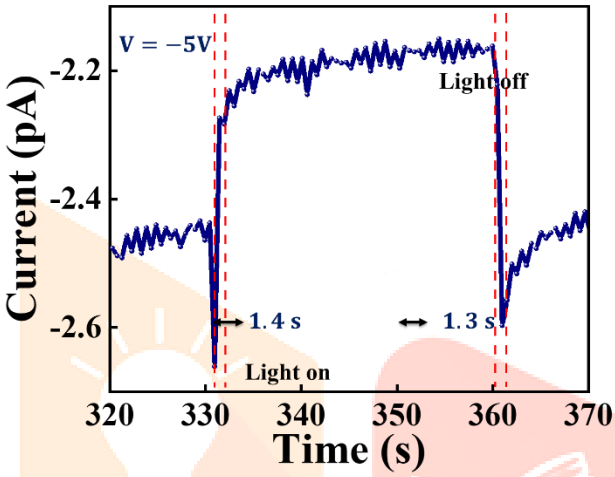

Fig. 5: Time-dependent photocurrent of the GaSe device subjected to periodic ON/OFF illumination cycles.

For our GaSe devices, the linear power scaling ($\alpha \approx 1$) and relatively fast response suggest moderate gain , balancing sensitivity with
speed [28,34].

IV. CONCLUSION

We have successfully demonstrated high-performance photodetectors based on mechanically exfoliated few-layer Gallium Selenide (GaSe) nanoflakes in a Metal–Semiconductor–Metal (MSM) architecture with engineered Schottky contacts. Through comprehensive structural, optical, and optoelectronic characterization, we have established several key findings. Raman and photoluminescence spectroscopy confirm that the exfoliated GaSe flakes exhibit excellent crystalline quality with characteristic vibrational modes and a direct optical bandgap at ~ 2.0 eV, ideal for visible-light photodetection. The strategic use of Schottky contacts in the MSM configuration effectively suppresses dark current to the order of 10^{-10} A at low bias, resulting in high signal-to-noise ratio. Analysis of the dark I–V characteristics yields a Schottky barrier height of $\Phi_B \approx 0.6$ eV and an Ideality factor of $\eta \approx 1.2$, confirming high-quality metal–semiconductor interfaces. Power-dependent photocurrent measurements reveal a linear power scaling relationship with $\alpha \approx 1$, extending across nearly three orders of magnitude in optical power. This result is a definitive signature of trap-free, efficient carrier transport, indicating that photogenerated carriers are collected without significant trapping or non-radiative recombination. This finding positions GaSe among the best-performing 2D photodetector materials in terms of intrinsic carrier dynamics. The devices exhibit strong photoresponse across the UV–visible–NIR spectrum, with peak responsivity of 17.5 A/W in the visible range. The spectral cutoff around 650–700 nm is consistent with the direct bandgap, confirming the band-to-band photodetection mechanism. The estimated external quantum efficiency of 3500% and detectivity of $\sim 10^{13}$ Jonesare competitive with state-of-the-art 2D material photodetectors. The combination of low dark current, efficient carrier transport, and broadband response makes GaSe an excellent candidate for applications including imaging, optical communication, environmental sensing, and

integrated optoelectronics. As the field of 2D materials continues to mature, GaSe stands out as a versatile, high-performance platform poised to play a central role in future photonic and optoelectronic technologies.

CONFLICT OF INTEREST

The author declares no conflicts of interest regarding the publication of this paper.

ACKNOWLEDGMENT

The author gratefully acknowledges the Department of Physics at Godda College, Sido-Kanhu Murmu University, for providing the academic environment to support this research. Sincere thanks are also extended to the Indian Institute of Technology (IIT) Delhi for providing the advanced experimental and characterization facilities where the foundational research and measurements for this work were conducted.

REFERENCES

[1] F. H. L. Koppens, T. Mueller, Ph. Avouris, A. C. Ferrari, M. S. Vitiello, and M. Polini, "Photodetectors based on graphene, other two-dimensional materials and hybrid systems," *Nat. Nanotechnol.* **9**, 780–793 (2014). DOI: 10.1038/NNANO.2014.215

[2] Q. H. Wang, K. Kalantar-Zadeh, A. Kis, J. N. Coleman, and M. S. Strano, "Electronics and optoelectronics of two-dimensional transition metal dichalcogenides," *Nat. Nanotechnol.* **7**, 699–712 (2012). DOI: 10.1038/nnano.2012.193

[3] K. S. Novoselov, A. K. Geim, S. V. Morozov, D. Jiang, Y. Zhang, S. V. Dubonos, I. V. Grigorieva, and A. A. Firsov, "Electric field effect in atomically thin carbon films," *Science* **306**, 666–669 (2004). DOI: 10.1126/science.1102896

[4] K. F. Mak, C. Lee, J. Hone, J. Shan, and T. F. Heinz, "Atomically thin MoS_2: A new direct-gap semiconductor," *Phys. Rev. Lett.* **105**, 136805 (2010). DOI: 10.1103/PhysRevLett.105.136805

[5] B. Radisavljevic, A. Radenovic, J. Brivio, V. Giacometti, and A. Kis, "Single-layer MoS_2 transistors," *Nat. Nanotechnol.* **6**, 147–150 (2011). DOI: 10.1038/nnano.2010.279

[6] L. Li, Y. Yu, G. J. Ye, Q. Ge, X. Ou, H. Wu, D. Feng, X. H. Chen, and Y. Zhang, "Black phosphorus field-effect transistors," *Nat. Nanotechnol.* **9**, 372–377 (2014). DOI: 10.1038/nnano.2014.35

[7] H. Liu, A. T. Neal, Z. Zhu, Z. Luo, X. Xu, D. Tománek, and P. D. Ye, "Phosphorene: An unexplored 2D semiconductor with a high hole mobility," *ACS Nano* **8**, 4033–4041 (2014). DOI: 10.1021/nn501226z

[8] S. Cai, J. Cen, J. Zuo, et al., "Research progress on the application of two-dimensional layered semiconductors in optoelectronic devices," *Appl. Comput. Eng.* **60**, 20240826 (2024). DOI: 10.54254/2755-2721/60/20240826

[9] Q. Lv, F. Chen, Y. Xia, and W. Su, "Recent progress in fabrication and physical properties of 2D TMDC-based multilayered vertical heterostructures," *Electronics* **11**, 2401 (2022). DOI: 10.3390/electronics11152401

[10] W. Jie, W. Jie, and J. Hao, "Two-dimensional layered gallium selenide: preparation, properties, and applications," in *Synthesis, Modeling, and Characterization of 2D Materials and Their Heterostructures* (Wiley, 2016), Ch. 1. DOI: 10.1002/9781119242635.CH1

[11] D. J. Late, B. Liu, H. S. S. Ramakrishna Matte, V. P. Dravid, and C. N. R. Rao, "Hysteresis in single-layer MoS_2 field effect transistors," *ACS Nano* **6**, 5635–5641 (2012). DOI: 10.1021/nn301572c

[12] S. Sorifi, P. Aggarwal, and S. Kaushik, "Investigation of thickness-dependent optical and optoelectronic properties of mechanically exfoliated GaSe nanoflakes," *ACS Appl. Electron. Mater.* **5**, 1543–1551 (2023). DOI: 10.1021/acsaelm.2c01612

[13] P. J. Ko, A. Abderrahmane, T. Takamura, N.-H. Kim, and A. Sandhu, "Thickness dependence on the optoelectronic properties of multilayered GaSe based photodetector," *Nanotechnology* **27**, 325202 (2016). DOI: 10.1088/0957-4484/27/32/325202

[14] S. Sorifi, M. Moun, S. Kaushik, and R. Singh, "High-temperature performance of a GaSe nanosheet-based broadband photodetector," *ACS Appl. Electron. Mater.* **2**, 670–676 (2020). DOI: 10.1021/ACSAELM.9B00770

[15] Y. Cao, K. Cai, P. Hu, L. Zhao, T. Yan, W. Luo, X. Zhang, X. Wu, K. Wang, and H. Zheng, "Strong enhancement of photoresponsivity with shrinking the electrodes spacing in few layer GaSe photodetectors," *Sci. Rep.* **5**, 8130 (2015). DOI: 10.1038/SREP08130

[16] D. V. Rybkovskiy, A. V. Osadchy, and E. D. Obraztsova, "Transition from parabolic to ring-shaped valence band maximum in few-layer GaS, GaSe, and InSe," *Phys. Rev. B* **90**, 235302 (2014). DOI: 10.1103/PhysRevB.90.235302

[17] Y. Ma, Y. Dai, M. Guo, C. Niu, Y. Zhu, and B. Huang, "Evidence of the existence of magnetism in pristine VX_2 monolayers (X = S, Se) and their strain-induced tunable magnetic properties," *ACS Nano* **6**, 1695–1701 (2012). DOI: 10.1021/nn204667z
[18] K. Wang, "(Invited) Layered (III-Se) Photodetectors," *ECS Trans.* **34**, 2212 (2016). DOI: 10.1149/ma2016-02/34/2212
[19] J. Hu, X. Ouyang, N. Dai, and Q. Guo, "Photoresponse and noise characteristics of indium selenide photodetectors," *Opt. Mater. Express* **7**, 1373–1383 (2017). DOI: 10.1364/OME.7.001373
[20] R. K. Yadav, J. Kumar, R. Kumar, R. Singh, and J. Dwivedi, "High performance broadband photodetector based on MoS_2/HfS_2 van der Waals heterostructure," *Appl. Surf. Sci.* **573**, 151552 (2022). DOI: 10.1016/j.apsusc.2021.151552
[21] S. M. Sze and K. K. Ng, *Physics of Semiconductor Devices*, 3rd ed. (Wiley-Interscience, Hoboken, NJ, 2006), Chapter 3.
[22] J. Jiang, C. Ling, T. Xu, W. Wang, and X. Niu, "Defect engineering for modulating the trap states in two-dimensional photoconductor," arXiv:1808.06198 (2018).
[23] W. Zhang, C.-P. Chuu, J.-K. Huang, C.-H. Chen, M.-L. Tsai, Y.-H. Chang, C.-T. Liang, Y.-Z. Chen, Y.-L. Chueh, J.-H. He, M.-Y. Chou, and L.-J. Li, "Ultrahigh-gain photodetectors based on atomically thin graphene-MoS_2 heterostructures," *Sci. Rep.* **4**, 3826 (2014). DOI: 10.1038/srep03826
[24] D. Jariwala, V. K. Sangwan, D. J. Late, J. E. Johns, V. P. Dravid, T. J. Marks, L. J. Lauhon, and M. C. Hersam, "Band-like transport in high mobility unencapsulated single-layer MoS_2 transistors," *Appl. Phys. Lett.* **102**, 173107 (2013). DOI: 10.1063/1.4803920
[25] W. Liu, J. Kang, D. Sarkar, Y. Khatami, D. Jena, and K. Banerjee, "Role of metal contacts in designing high-performance monolayer n-type WSe_2 field effect transistors," *Nano Lett.* **13**, 1983–1990 (2013). DOI: 10.1021/nl304777e
[26] G. Konstantatos, M. Badioli, L. Gaudreau, J. Osmond, M. Bernechea, F. P. Garcia de Arquer, F. Gatti, and F. H. L. Koppens, "Hybrid graphene-quantum dot phototransistors with ultrahigh gain," *Nat. Nanotechnol.* **7**, 363–368 (2012). DOI: 10.1038/nnano.2012.60
[27] A. Allain, J. Kang, K. Banerjee, and A. Kis, "Electrical contacts to two-dimensional semiconductors," *Nat. Mater.* **14**, 1195–1205 (2015). DOI: 10.1038/nmat4452
[28] Q. Zhao, W. Wei, F. Carrascoso-Plana, W. Jie, T. Wang, A. Castellanos-Gomez, and R. Frisenda, "The role of traps in the photocurrent generation mechanism in thin InSe photodetectors," *Mater. Horiz.* **7**, 252–262 (2020). DOI: 10.1039/C9MH01020C
[29] Y. Zhang, Y. Zheng, K. Rui, H. H. Hng, K. Hippalgaonkar, J. Xu, W. Sun, J. Zhu, Q. Yan, and W. Huang, "2D black phosphorus for energy storage and thermoelectric applications," *Small* **13**, 1700661 (2017). DOI: 10.1002/smll.201700661
[30] B. Sun, J. Xu, M. Zhang, L. He, and H. Zhu, "Progress on crystal growth of two-dimensional semiconductors for optoelectronic applications," *Crystals* **8**, 252 (2018). DOI: 10.3390/CRYST8060252
[31] P. Blake, E. W. Hill, A. H. Castro Neto, K. S. Novoselov, D. Jiang, R. Yang, T. J. Booth, and A. K. Geim, "Making graphene visible," *Appl. Phys. Lett.* **91**, 063124 (2007). DOI: 10.1063/1.2768624
[32] A. C. Ferrari, J. C. Meyer, V. Scardaci, C. Casiraghi, M. Lazzeri, F. Mauri, S. Piscanec, D. Jiang, K. S. Novoselov, S. Roth, and A. K. Geim, "Raman spectrum of graphene and graphene layers," *Phys. Rev. Lett.* **97**, 187401 (2006). DOI: 10.1103/PhysRevLett.97.187401
[33] C. R. Dean, A. F. Young, I. Meric, C. Lee, L. Wang, S. Sorgenfrei, K. Watanabe, T. Taniguchi, P. Kim, K. L. Shepard, and J. Hone, "Boron nitride substrates for high-quality graphene electronics," *Nat. Nanotechnol.* **5**, 722–726 (2010). DOI: 10.1038/nnano.2010.172
[34] O. Lopez-Sanchez, D. Lembke, M. Kayci, A. Radenovic, and A. Kis, "Ultrasensitive photodetectors based on monolayer MoS_2," *Nat. Nanotechnol.* **8**, 497–501 (2013). DOI: 10.1038/nnano.2013.100
[35] H. S. Nalwa, "A review of molybdenum disulfide (MoS_2) based photodetectors: from ultra-broadband, self-powered to flexible devices," *RSC Adv.* **10**, 30529–30602 (2020). DOI: 10.1039/D0RA03183F